energies

MDPI

Article

Pawpaw (*Carica papaya*) Peel Waste as a Novel Green Heterogeneous Catalyst for Moringa Oil Methyl Esters Synthesis: Process Optimization and Kinetic Study

Babatunde Oladipo [1,2], Tunde V Ojumu [2], Lekan M Latinwo [3] and Eriola Betiku [1,3,*]

1 Biochemical Engineering Laboratory, Department of Chemical Engineering, Obafemi Awolowo University, Ile-Ife 220005, Osun State, Nigeria; btoladipo@gmail.com
2 Department of Chemical Engineering, Cape Peninsula University of Technology, Bellville Campus, Symphony Way, Bellville, Cape Town 7535, South Africa; OjumuT@cput.ac.za
3 Department of Biological Sciences, Florida Agricultural and Mechanical University, Tallahassee, FL 32307, USA; lekan.latinwo@famu.edu
* Correspondence: eriola.betiku@famu.edu

Received: 3 October 2020; Accepted: 29 October 2020; Published: 9 November 2020

Abstract: This study evaluated pawpaw (*Carica papaya*) peel ash as a green solid base catalyst for *Moringa oleifera* oil methyl esters (MOOME) production. Taguchi orthogonal array approach was used to examine the impact of vital process input variables (calcined pawpaw peel (CPP) loading, reaction temperature, methanol-to-*M. oleifera* oil (MeOH:MOO) molar ratio and reaction time) on the MOOME yield. Catalytic potency potential of the CPP was evaluated by Fourier transform infrared (FTIR), Barrett-Joyner-Halenda (BJH), Brunauer-Emmett-Teller (BET), scanning electron microscope (SEM), energy-dispersive X-ray spectroscopy (EDX) and X-ray diffraction (XRD) methods. The results obtained indicate that the CPP consists of nanoparticles and alkaline elements K (23.89 wt.%), Ca (2.86 wt.%) and Mg (1.00 wt.%). The high values of coefficient of determination, R^2 (0.9992) and adjusted R^2 (0.9968) as well as the low value of the coefficient of variation (0.31%) for the model developed indicate it can be used to sufficiently describe the transesterification process. MOOME yield of 96.43 ± 0.10 wt.% was achieved at the optimum values of 3.5 wt.% CPP loading, 9:1 MeOH:MOO molar ratio, 35 °C reaction temperature and 40 min reaction time. The kinetic modeling of the transesterification process determined the reaction rate constant and overall reaction order as 0.20465 $L{\cdot}mol^{-1}{\cdot}s^{-1}$ and 2, respectively. The results of this study demonstrate both CPP and MOO are feasible renewable resources for MOOME production. The kinetic data generated may be useful in reactor design for the transesterification process.

Keywords: plant oil; agricultural waste; catalyst; Taguchi method; biodiesel; kinetics

1. Introduction

The negative impact of global warming and the exhaustive nature of petroleum fuels are driving the quest for alternative fuels that are environmentally friendly and sustainable. Fatty acid methyl esters (FAME), generally called biodiesel, which is developed from plant oils, animal fats, lipids from microalgae and waste oils, has been suggested as a potential candidate. The utilization of FAME as a fuel offers various benefits such as renewability, sustainability and high energy return. It is non-toxic and environmentally benign as it lowers the emission of carbon dioxide and harmful compounds, namely, sulfur, NO_x and particulate matter [1,2].

Various types of oils have been assessed for FAME production, ranging from the first generation fuel, which is derived from edible oils such as palm oil [3], sunflower oil [4] and soybean oil [5]; the second generation fuel, which comprises non-edible oils such as castor oil [6], neem oil [7], jatropha oil [8], Philippine tung oil [9], kapok oil [10], honne oil [11], sandbox oil [12] and used cooking oil [13]; and the third generation fuel, which consists of microalgae-based lipids [14]. Although plant oils are a sustainable energy source with energy contents near that of petro-diesel, they cannot be utilized directly as fuel in internal combustion engines because of the high free fatty acid (FFA) and viscosity contents in addition to their ability to form gum [15].

Plant oils are used as raw material for the production of FAME via the transesterification process in the presence of a catalyst, which can either be homogeneous or heterogeneous. When compared with heterogeneous-catalyzed transesterification processes, homogeneous-catalyzed ones are moderately faster and display higher conversion with minimal side reactions, but they cannot compete with petro-diesel in terms of cost [16,17]. Moreover, homogeneous catalysts cannot be recovered and reused. The FAME produced has to be purified, the generation of a large quantity of wastewater to neutralize and separate them from the methyl esters phase at the end of the reaction is another shortcoming of using homogeneous catalysts. Thus, heterogeneous catalysis has been suggested as a replacement for the conventional homogeneous catalysis [1]. The ease of separating heterogeneous catalysts from the product mixture by simple filtration helps in its reusability for further production. Therefore, the application of solid catalysts in place of homogeneous catalysts could promote a cost-effective FAME production process and also prevent environmental pollution.

The current attention on catalyst application for FAME production is being directed towards the synthesis of novel green solid catalysts derived from wastes-based natural sources. Green catalysts derived from waste biomass and investigated for the production of FAME via transesterification include coconut husk [8], flamboyant pod [18], banana peel [19–21], cocoa pod husks [7], rubber seed shell [22], tucumã peels [23], pomelo peel [24] and ripe plantain peels [25].

Pawpaw (*Carica papaya*) could serve as a source of green catalyst for the transesterification of oil and alcohol. Pawpaw is the most economically important fruit in the *Caricaceae* family, which is believed to have originated from southern Mexico and neighboring Central America [26]. It serves as a rich source of antioxidant nutrients, B vitamins, minerals and fiber as well as the source of the digestive enzyme papain [27]. There has been an increase in global pawpaw production in recent years due to a jump in market demand for tropical fruits. The world production of pawpaw was estimated to be 13.29 million tons in 2018 and Nigeria is the 6th largest producer globally with an estimated production of 0.83 million tons in the same year [28]. Figure 1 shows pawpaw production share by region in 2018. Typical pawpaw has a percentage composition of 8.5% seed, 12% skin and 79.5% pulp [26].

The disposal of the fairly tough waxy skin (peel) waste is a major concern. Since the peel is not consumable, as it can lead to stomach irritation, value-addition to the peel as a source of base heterogeneous catalyst will help solve its disposal problem and make FAME production cost-effective. Although the use of pawpaw peel as a source of heterogeneous catalyst has not been reported, the effectiveness of the heterogeneous catalyst prepared using pawpaw stem in C-C bond formation and biodiesel production via transesterification has been demonstrated [29].

Moringa oleifera is a member of the genus Moringaceae. It is a highly valued plant that is versatile, adaptable, easy to cultivate and self-propagating with fast growth rate. By weight, the seed has approximately 42% of oil; thus, it can be used as a potential feedstock for biodiesel production [30]. There are various reports on biodiesel production from moringa oil using both homogeneous [31–35] and heterogeneous [36–39] catalysts. However, none of these studies investigated the kinetics of the transesterification process used. The most attractive property of biodiesel derived from *M. oleifera* oil is the high cetane numbers of above 60, which are among the highest reported for biodiesel [31].

This present study was aimed at preparing an active heterogeneous catalyst from pawpaw peel, which was applied to the conversion of *Moringa oleifera* oil (MOO) to FAME. The transesterification process was modeled and optimized using the Taguchi orthogonal array design method, which allows

for a smaller number of experiments compared to response surface methodology involving Box-Behnken and central composite designs. Additionally, the kinetic modeling of the transesterification process for the fatty esters production was undertaken to estimate pertinent parameters, i.e., reaction constant and overall kinetic reaction order.

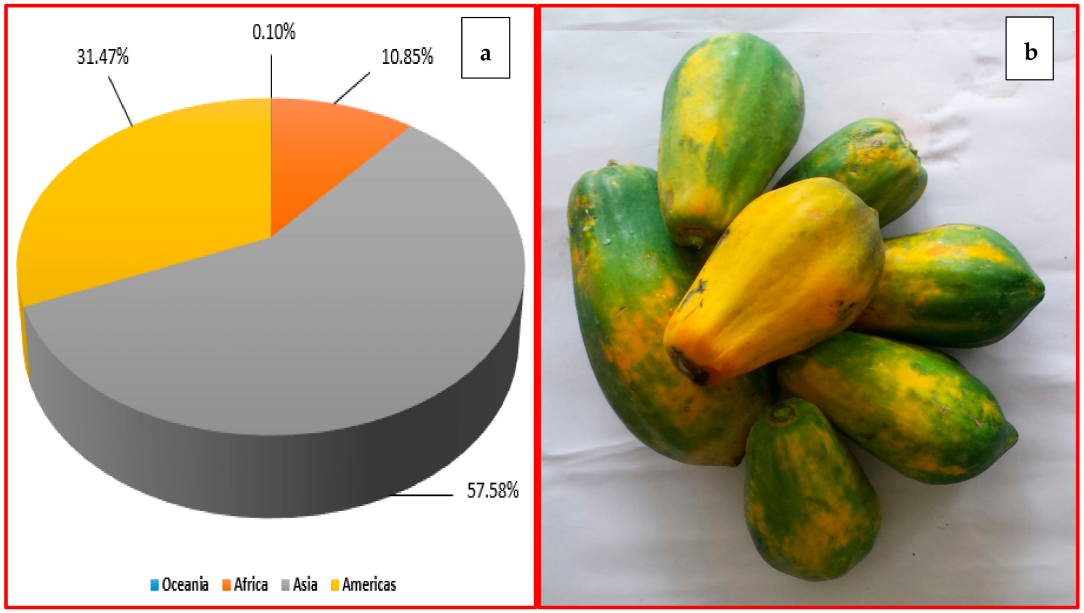

Figure 1. Pawpaw production share by region (**a**) in 2018 and pawpaw image (**b**).

2. Materials and Methods

2.1. Moringa Oil and Other Chemicals

The pawpaw peel utilized in this study was collected between September and October 2017 from Odurain Village, Ile-Ife, Osun State, which is situated at a longitude of 4.5667° E and latitude of 7.4667° N, Southwestern Nigeria. The extraction, fatty acid composition and the physiochemical properties of the MOO used have been described in our previous work [30]. All chemicals and reagents used were of analytical grade and were supplied by a local retailer and used without further purification.

2.2. Methods

Catalyst Preparation

The pawpaw peel collected was first sliced into small sizes to quicken the drying operation. The peel was rinsed with tap water to remove sand and organic contaminants adhering to it and dried in the sun for 7 days. To reduce the carbon content, the sun-dried peel was then burned in open-air to generate ash which was ground to powder and allowed to cool. The powder obtained was sieved through an 0.8 mm Endecott sieve to produce fine ash. Heat treatment of the fine-powered ash via calcination was conducted in a muffle single-chamber furnace (Carbolite^{TM} AAF 11/7) by investigating the effect of temperature between 200 and 1000 °C for 4 h. The calcined samples were thereafter stored in corked tubes and kept in a desiccator for further use [19,25].

2.3. Catalyst Characterization

2.3.1. Potency Test of Catalyst Developed

Fourier transform infrared (FTIR), Barrett–Joyner–Halenda (BJH), Brunauer–Emmett–Teller (BET), scanning electron microscope (SEM), energy-dispersive X-ray spectroscopy (EDX) and X-ray

diffraction (XRD) analyses were carried out to examine the nature of the synthesized catalyst (calcined pawpaw peel (CPP)). The surface structure and morphological features of the prepared CPP were viewed under a high-resolution FEI Nova NanoSEM230 enhanced with a field emission gun and coupled with EDX. Elemental composition analysis was performed at 10 keV with an Oxford X-Max 20 mm^2. Surface functional groups present in the CPP were examined via an FTIR spectrophotometer (Thermo-Nicolet iS10) enhanced with attenuated total reflectance using a scale of 4000−400 cm^{-1}. The crystalline nature of the CPP was studied on a D8 Advance diffractometer (Bruker AXS, Karlsruhe, Germany) with Cu Kα radiation (λKα1 = 1.5406 Å) fitted with a LynxEye position-sensitive detector. Physisorption analysis of the CPP was investigated using N_2 adsorption-desorption isotherm at liquid N_2 temperature of −196 °C with Micromeritics TriStar II 3020 (Version 2.00). Determination of the pore diameter and pore size distribution from adsorption isotherms were performed by the BJH technique. The calculation of the specific surface area was conducted using the BET method. Before any measurement, the degassing of samples was carried out overnight in an oven at a temperature of 393 K under vacuum to eliminate dampness [19,25].

2.3.2. Experimental Design and Data Analysis for MOOME Production

For the transesterification process, the Taguchi design method was employed in generating the experimental conditions used in this work by selecting four essential input variables (CPP loading 2–5 wt.%, MeOH:MOO molar ratio 3:1–15:1, reaction time 40–80 min and reaction temperature 35–65 °C), which were investigated at three different levels. The number of experiments was determined by Equation (1). Nine experimental conditions were generated in this work.

$$N = P(L-1) + 1 \quad (1)$$

where N is the total number of experiments, P is the number of process input variables considered and L is the level selected.

A mathematical regression model was developed to predict the MOOME yield using the results obtained from the laboratory. The influence of each process variable was examined by determining the impact level on the MOOME yield using Equation (2). The optimum values suggested by the mathematical model were verified by a confirmatory experiment that was carried out in triplicate in the laboratory. The impact of each process input variable on the MOOME yield in the regression model developed was investigated using analysis of variance (ANOVA) technique. Design-Expert version 10.0 (Stat-Ease Inc., Minneapolis, MN, USA) software was employed for this work.

$$\text{Impact factor } (\%) = \frac{\text{Sum of squares of each factor}}{\text{Sum of squares for all factors}} \quad (2)$$

The statistical analysis of the model developed for the transesterification process was assessed by analysis of variance (ANOVA) and the efficacy of the model was further checked by the coefficient of determination (R^2), adjusted R^2, predicted R^2, signal-to-noise ratio (SNR), standard deviation (S.D.), mean and coefficient of variance (CV).

2.3.3. Transesterification of MOO to MOOME

The initial FFA content of the MOO used in this study was 1.44%, which will promote the saponification reaction over the desired transesterification reaction, leading to soap formation and difficulty in the separation of products. Hence, a two-step (acid-base) catalyzed transesterification process was used to convert the MOO into MOOME. First, the modified method of Ighose et al. [40] was used for the esterification process. The condition used to reduce the FFA content to 0.59% was a temperature of 65 °C, methanol-to-oil molar ratio of 9:1, H_2SO_4 loading of 3 wt.% and 40 min of reaction time. For the second step, the procedure described in our previous report was used [19]. The batch process for the reaction was conducted in a 250 mL round-bottom flask with two necks coupled with a

condensing system on one end and the other end was used for sampling. According to the different sets of process input variables used (Table 1), the esterified MOO and methanol were charged into the flask and the CPP was introduced to the oil-methanol mixture. On the completion of each experiment at a specified time, the resulting product mixture was transferred into centrifuge tubes and fractions were separated at 8000 rpm for 5 min. After centrifugation, the spent solid catalyst attached to the bottom of the centrifuge tubes and the liquid mixture separated into two layers; biodiesel layer (MOOME) and glycerol layer. The MOOME produced was then separated from the glycerol layer and transferred into a separating funnel for further purification by washing with warm distilled water (50 °C) to remove entrained glycerol, catalyst, methanol and soap until a clear solution of water appeared. Sodium sulphate was used as a drying agent to remove the water left in the washed MOOME. The yield of MOOME produced was determined by Equation (3):

$$\text{MOOME (wt.\%)} = \frac{\text{Weight of MOOME produced}}{\text{Weight of MOO used}} \quad (3)$$

Table 1. Experimental design matrix generated by L_9 orthogonal array with MOOME yield.

Run Number	Variables and Their Levels				Experimental MOOME Yield (wt.%)
	MeOH:MOO Molar Ratio	CPP Loading (wt.%)	Reaction Temperature (°C)	Reaction Time (min)	
1	3	2	35	40	91.65
2	15	2	65	60	82.4
3	9	2	50	80	89.19
4	15	5	50	40	83.22
5	15	3.5	35	80	84.6
6	9	3.5	65	40	96.36
7	3	3.5	50	60	94.08
8	9	5	35	60	90.58
9	3	5	65	80	87.13

2.3.4. Kinetic Modeling

In this work, the kinetic modeling of the transesterification process was developed using the optimal condition established for the process. A detailed description of the method used for the modeling by investigating eight kinetic scenarios is described in our earlier work [41,42]. In determining the reaction order, the values of MOO conversion were used in the linear mathematical equations under the eight scenarios considered, then, the *x-y* plot was drawn using the variables and its coefficient of determination (R^2) was evaluated. The slope of the fitted line represents the pertinent kinetic parameter known as the rate constant (k) of the reaction. R^2 of the eight scenarios were examined and the one with the highest value was taken as the overall order of the reaction. OriginPro 2018 (OriginLab Corp., Northampton, MA) software was used to fit the average of MOOME yields and the kinetic plots.

3. Results and Discussion

3.1. Analyses of Catalyst Developed from Pawpaw Peels

3.1.1. SEM/EDX Characterization of CPP

Textural structures of the raw pawpaw peel (RPP) and CPP viewed from the SEM and EDX images are depicted in Figure 2a,b. The image of the raw sample shows that it has a solid irregular surface, while the presence of jointed light-tiny strips with pores is observed in the CPP. Upon calcination, the size reduction of the particles was observed, and the shape of the particles became more structured, which led to the porous and spongy attributes of the ash fragments. This corroborates the sintered form of small metallic clusters to yield agglomerative particles of the calcined catalyst [19,43]. Furthermore,

a fine powder form of crystals was observed after calcination, which may also be responsible for its high catalytic activity due to increased surface area [44].

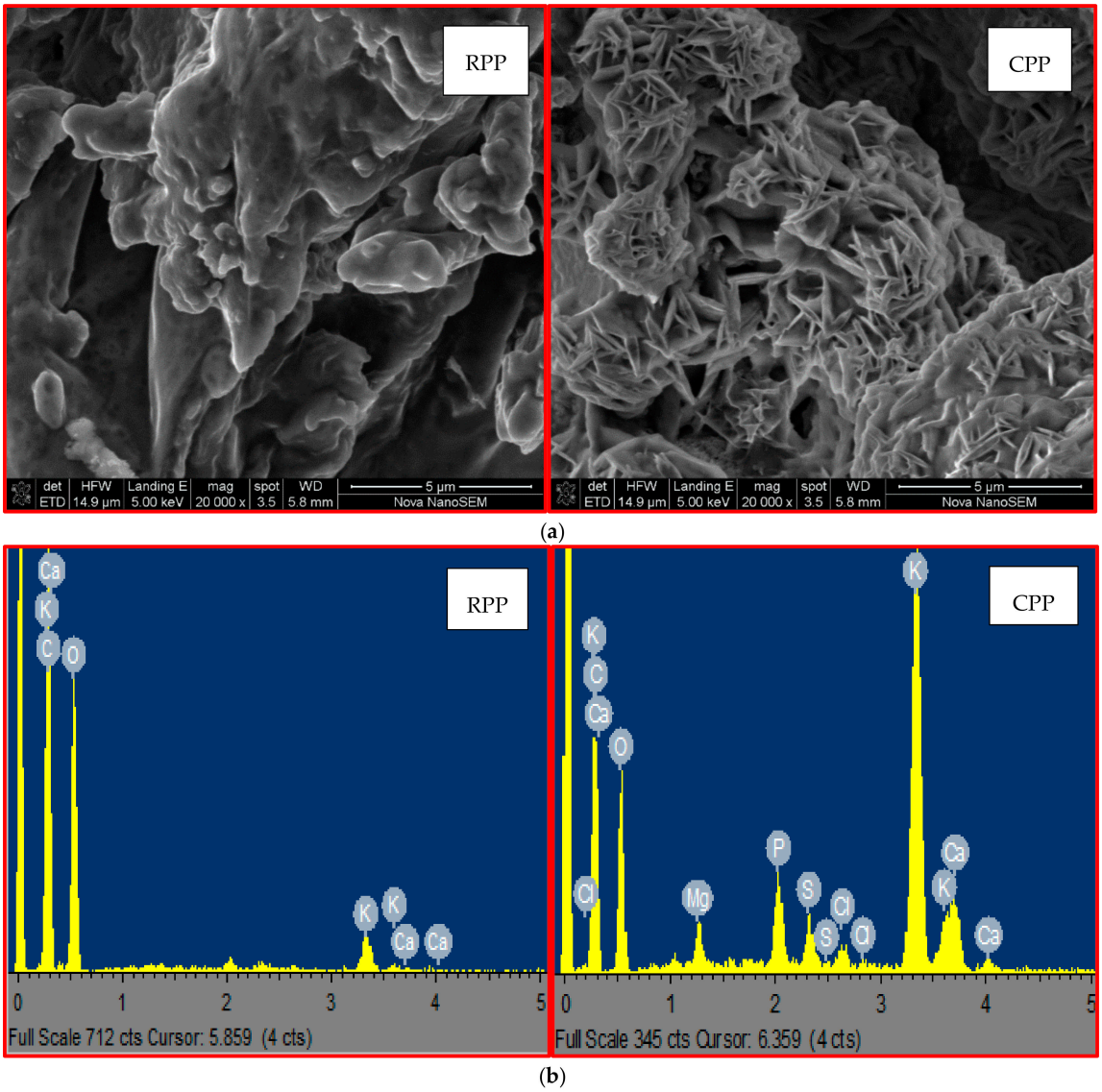

Figure 2. Plots of (**a**) SEM and (**b**) EDX images of RPP and CPP (at 600 °C) samples.

The elemental composition obtained from the EDX results of the raw and calcined samples of the peel are presented in Table 2. Major metallic elements detected in the calcined sample at 600 °C were Mg, K and Ca with a cumulative mass fraction of 27.75%. Thus, large-scale production of the CPP ash was produced at 600 °C for use in the MOOME production. It has been shown by EDX analysis that pawpaw peel ash contains oxides of K, Ca, Mg and Na, while water-extract of the ash analyzed by ion-exchange chromatography and flame photometry showed K as the main metal present [45]. Additionally, it has been demonstrated that K is mainly responsible for the catalytic activity of some catalysts produced from biomass wastes such as pawpaw stem calcined [29], banana peels [19], *Sesamum indicum* plant [46] and plantain peels [47]. Observation from the EDX analysis showed that the application of controlled heat on the pawpaw peel ash positively affected its catalytic prospect. Moreover, it has been noted that calcination helps alkali elements in maintaining their strong potentials in the transesterification process [48].

Table 2. EDX analysis results of CPP.

Heat (°C)	Composition (%)										
	C	O	Mg	P	S	Cl	K	Ca	Fe	Na	Si
RPP	56.81	41.86	0.00	0.00	0.00	0.00	1.16	0.17	0.00	0.00	0.00
200	46.59	28.37	1.26	2.81	2.57	0.64	14.75	3.01	0.00	0.00	0.00
400	32.32	36.33	1.67	3.62	2.15	0.59	20.37	2.95	0.00	0.00	0.00
600	29.16	36.72	1.00	3.04	2.45	0.87	23.89	2.86	0.00	0.00	0.00
800	40.85	32.86	0.43	1.62	2.34	0.63	19.26	0.00	1.63	0.37	0.00
1000	18.40	46.16	0.00	2.91	2.59	0.00	24.41	3.09	0.00	0.95	1.50

3.1.2. FTIR Analysis of CPP

The spectrum obtained for the CPP at 600 °C is shown in Figure 3. In comparison to the RPP (spectrum not shown), major transformations occurred in the spectrum of the CPP. A relatively narrow, weak-to-moderate absorption band located at 1650 cm^{-1} shows the presence of olefinic unsaturation (C=C) in the sample [49]. The narrow medium intensity out-of-plane band vibration mode observed at 880 cm^{-1} is associated with CO_3^{2-} species and this explains the presence of K_2CO_3 noticeable at a wavelength of 1388 cm^{-1}. This well-defined band is due to a strong interaction between CO_2 and specific basic sites on the catalyst surface [21,49,50], signifying the catalytic potential of the CPP in a transesterification process. Additionally, the medium to strong bands in the range 1110–1025 cm^{-1} presented an elementary hydrogen-bonded OH absorption of a hydroxyl function [49].

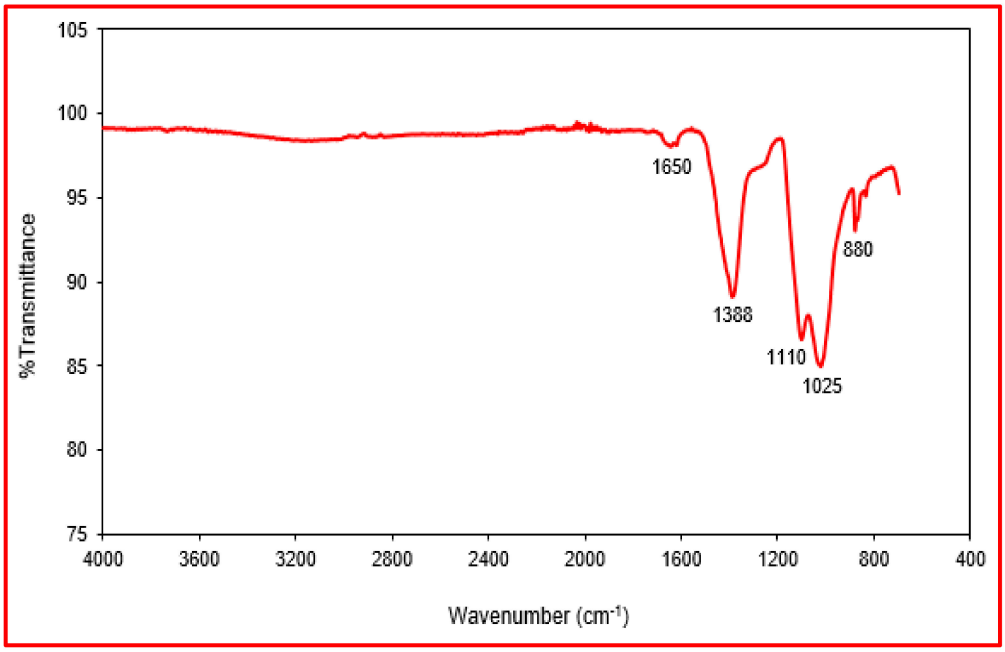

Figure 3. Fourier transform infrared (FTIR) spectrum of CPP at 600 °C.

3.1.3. XRD Analysis of CPP

Figure 4 shows the XRD pattern observed for the CPP at 600 °C. The diffraction peaks located at 2θ values of 32.26. 39.63, 44.84 and 47.82 degrees are attributed to the presence of $K_2CO_3.1.5H_2O$ in the CPP sample. In addition, peaks located at 2θ values of 23.92, 29.85, 30.92, 56.22 and 59.74 degrees confirm the presence of K_2SO_4, while peaks found at 2θ values of 28.26, 40.67, 50.21, 66.24 and 74.88 degrees are ascribed to KCl.

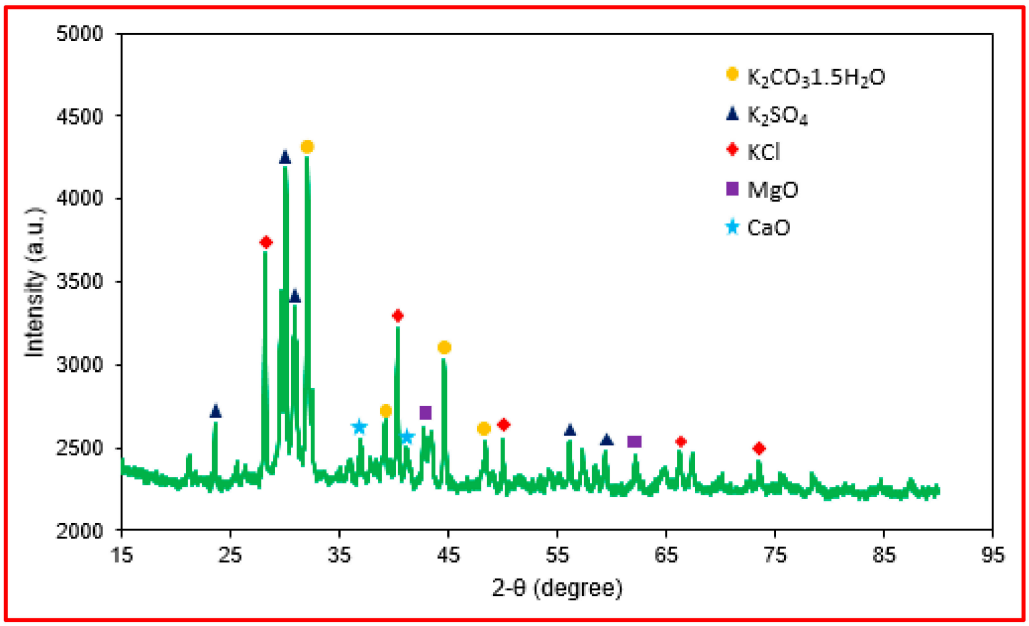

Figure 4. X-ray diffraction (XRD) pattern of CPP at 600 °C.

The presence of MgO is confirmed by the peaks located at 2θ values of 43.66 and 62.92 degrees, while the presence of CaO is attributable to the peaks identified at 2θ values of 36.42 and 41.35 degrees. The compounds found in the CPP have been reported in work done on other waste biomass, such as plantain peels [25], banana peel [19–21], kesseru [51], activated wood [48] and the mixture of plantain peel, kola nut pod husk and cocoa pod husk [52]. In particular, the presence of K_2CO_3, K_2SO_4 and KCl were reported in pawpaw stem calcined at 700 °C for 4 h [29]. The presence of K_2CO_3, K_2SO_4, KCl and MgO were also observed in waste *Sesamum indicum* plant calcined at 550 °C for 2 h [46]. The findings in the XRD pattern agree with the results of EDX and FTIR.

3.1.4. Physisorption Analysis of CPP

Figure 5a shows the N_2 adsorption-desorption isotherm of CPP, which displays a conventional type IV characteristic curve and hysteresis loop type H3 indicating the mesoporous nature of the catalyst [29,53,54]. The surface area of the CPP catalyst calcined at 600 °C was measured as 3.6042 m^2/g with corresponding mean pore diameter and pore volume of 8.54 nm and 0.00706 cm^3/g, respectively. From a physisorption perspective, pore width between 2 and 50 nm is termed mesopore [55]. As observed in the corresponding pore size distribution curve (Figure 5b), the bulk of the mean pore sizes are within this threshold, which confirmed that the CPP comprises mainly mesopores. This implies that there would be easy penetration of oil molecules into the CPP, thereby promoting transesterification process [56].

3.2. Regression Model for MOOME Production Process

Equation (4) depicts the mathematical regression model equation developed to predict the MOOME yield in terms of the coded factors:

$$R = 88.80 + 2.15A[1] + 3.24A[2] - 1.05B[1] + 2.88B[2] + 1.61D[1] + 0.22D[2] \quad (4)$$

where R is the response (MOOME yield, wt.%), A is the MeOH:MOO, B is the CPP loading (wt.%), D is the reaction time (min), $A[1]$ and $A[2]$ are the MeOH:MOO at 1st and 2nd levels, respectively, $B[1]$ and $B[2]$ are CPP loading at 1st and 2nd levels, respectively, and $D[1]$ and $D[2]$ are reaction time at 1st and 2nd level, respectively.

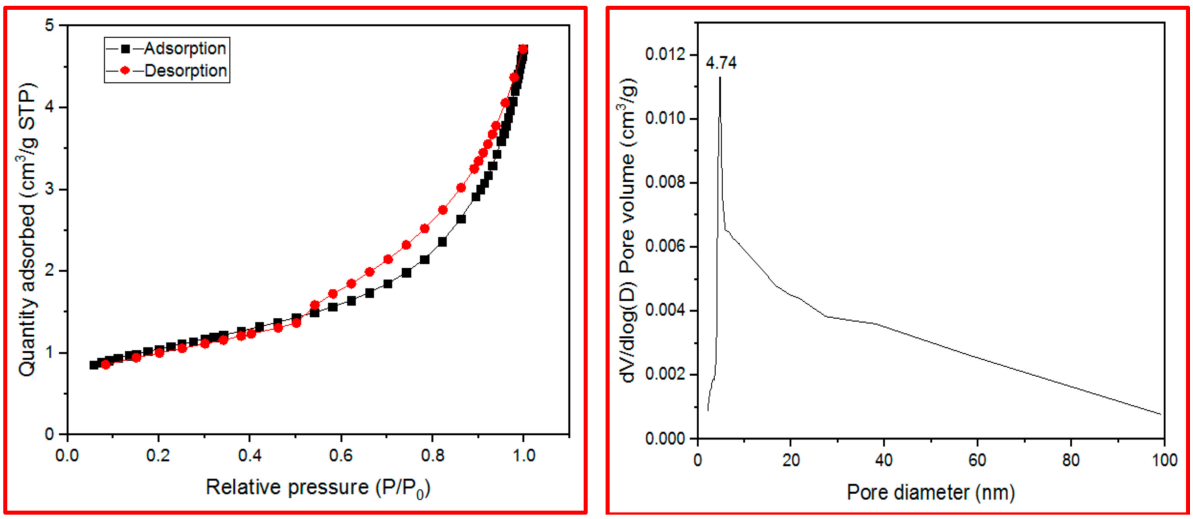

Figure 5. Plots of (**a**) N_2 adsorption/desorption isotherms and (**b**) pore-size distribution for CPP.

The significance level of the model terms on the yield and ANOVA results for the regression model are shown in Table 3. The combination of the F-value and *p*-value of a process input variable is used to determine its significance on the response. MeOH:MOO molar ratio, CPP loading and reaction time are the significant terms with *p*-value < 0.05. However, the reaction temperature was found to be insignificant, hence its omission from the regression model equation (Equation (4)). The impact of each process variable on the response was evaluated using Equation (2) and the results obtained revealed that the MOOME yield was mostly influenced by MeOH:MOO molar ratio with an impact factor of 70.28%, followed by CPP loading with a factor of 20.22% and reaction time with a factor of 9.49%. A high F-value of 416.82 and a low *p*-value of 0.0024 indicate the significance of the regression model.

Table 3. Statistics for the regression model for MOOME production process.

Source	ANOVA for the Model					Accuracy Test	
	SS	df	MS	F-Value	*p*-Value	Parameter	Value
Model	188.85	6	31.47	416.82	0.0024	Standard deviation	0.27
A—MeOH:MOO	132.73	2	66.37	878.89	0.0011	Mean	88.80
B—CPP loading	38.19	2	19.09	252.85	0.0039	%CV	0.31
D—Reaction time	17.93	2	8.97	118.73	0.0084	R^2	0.9992
Residual	0.15	2	0.076			Adjusted R^2	0.9968
Total	189.00	8				Predicted R^2	0.9838
						SNR	57.604

SS—Sum of squares, df—degree of freedom, MS—mean square, CV—coefficient of variation, SNR—signal-to-noise ratio.

Other statistics used to test the accuracy of the model are shown in Table 3. The high R^2 means that 99.92% variation of the predicted MOOME yields could be elucidated by the model. This is supported by the high value observed for the adjusted R^2 (0.9968), a parameter that excludes the insignificant terms of the model [57]. The predicted R^2 and adjusted R^2 of the regression model agreement, with an acceptable difference of 0.013 (i.e., it is below the highest permitted difference of 0.2). A signal-to-noise ratio (SNR) of 57.60 was estimated for the model, which implies a sufficient signal of the model to control the design space. Usually, a value >4 is appropriate. The accuracy of the model was further established with low values of the coefficient of variance and standard deviation of 0.31% and 0.27, respectively.

3.3. Influence of Process Variables on MOOME Yield

MeOH:Oil molar ratio is a major parameter that influences biodiesel yield in a transesterification process. The impact of MeOH:MOO molar ratio on MOOME yield is represented in Figure 6a, while the other process variables were maintained at 3.5 wt.% CPP loading, 35 °C reaction temperature and 40 min reaction time. To shift the equilibrium forward, methanol is usually supplied in surplus of the stochiometric required amount [7,58]. Thus, three levels of MeOH:MOO molar ratio were investigated (3:1, 9:1 and 15:1). The MOOME yield slightly increased from 95.44 to 96.53% when MeOH:MOO molar ratio was increased from 3:1 to 9:1. But a further increase to 15:1 led to the reduction of the MOOME yield by 8.95%. This reduction observed in the yield may be because methanol as alcohol with a polar hydroxyl group can behave as an emulsifying agent when used in high proportion. Additionally, it has been shown that surplus methanol hinders glycerol separation leading to a decrease in biodiesel yield [18,59]. Lv et al. [60] observed a reduction of biodiesel yield from 88.1 ± 1.5% to 49.0 ± 0.8% when methanol-to-oil ratio was increased from 7:1 to 12:1, which was ascribed to the surplus methanol in the reaction system.

The influence of CPP loading on the MOOME yield is depicted in Figure 6b. The CPP loading was investigated at three levels (2, 3.5 and 5 wt.%), while other process variables were kept at MeOH:MOO molar ratio of 9:1, reaction temperature of 35 °C and reaction time of 40 min. MOOME yield of 96.53% was obtained at a corresponding 3.5 wt.% CPP loading, which increased from the initial yield of 92.60% at 2 wt.% of CPP loading. The increase of the CPP from 3.5 to 5 wt.% resulted in the reduction of the MOOME yield by 4.87%. This decrease in yield can be ascribed to the excess catalyst in the reaction system since surplus catalyst triggers more triglycerides to take part in saponification reaction, leading to the formation of soap and subsequent reduction in biodiesel yield. Additionally, a high dosage of the CPP may have increased the viscosity of reactants, thereby leading to biodiesel reduction [15,18,61].

The impact of reaction time on MOOME yield is illustrated in Figure 6c with other operating variables maintained at MeOH:MOO of 9:1, CPP loading of 3.5 wt.% and reaction temperature of 35 °C.

MOOME yield of 96.53% was observed at 40 min, which demonstrates that sufficient time was given to the reaction for equilibrium to be achieved. However, a reduction of 1.44% in the MOOME yield was observed when the reaction time was increased to 60 min and prolonging the reaction time to 80 min resulted in a further reduction in the yield. This negative impact on the yield with an increase in reaction time beyond the optimum may be linked to the reversible nature of the transesterification reaction, which causes difficulty in separating the products [62]. Additionally, extending the reaction time beyond the optimum leads to the hydrolysis of the esters, producing fatty acids instead of biodiesel [61].

3.4. Process Variables Optimization and Model Verification

All the operating variables were kept within the ranges investigated while setting a maximum goal for MOOME yield. The proposed optimal condition for the transesterification process by solving Equation (4) with the software was reaction temperature of 35 °C, MeOH:MOO molar ratio of 9:1, reaction time of 40 min and CPP loading of 3.5 wt.%, with the corresponding MOOME yield of 96.53%. The proposed optimal condition was verified by performing a laboratory experiment in triplicate using the suggested optimum values. The average MOOME yield obtained was 96.43%. The result agrees reasonably with the predicted MOOME yield of 96.53 ± 0.10%, showing that the regression model developed for the MOOME production process is adequate. Table 4 details a comparison of some heterogeneous catalyst characterization, process optimization and corresponding biodiesel yield through the transesterification process. The optimal condition established in this present study is superior to most of the listed work in Table 4. A low reaction temperature (35 °C), low reaction time (40 min), moderate catalyst loading (3.5 wt.%) and moderate MeOH:Oil molar ratio (9:1) coupled with a moderate synthesis condition for the CPP signal a potential low-cost biodiesel production process for the MOOME.

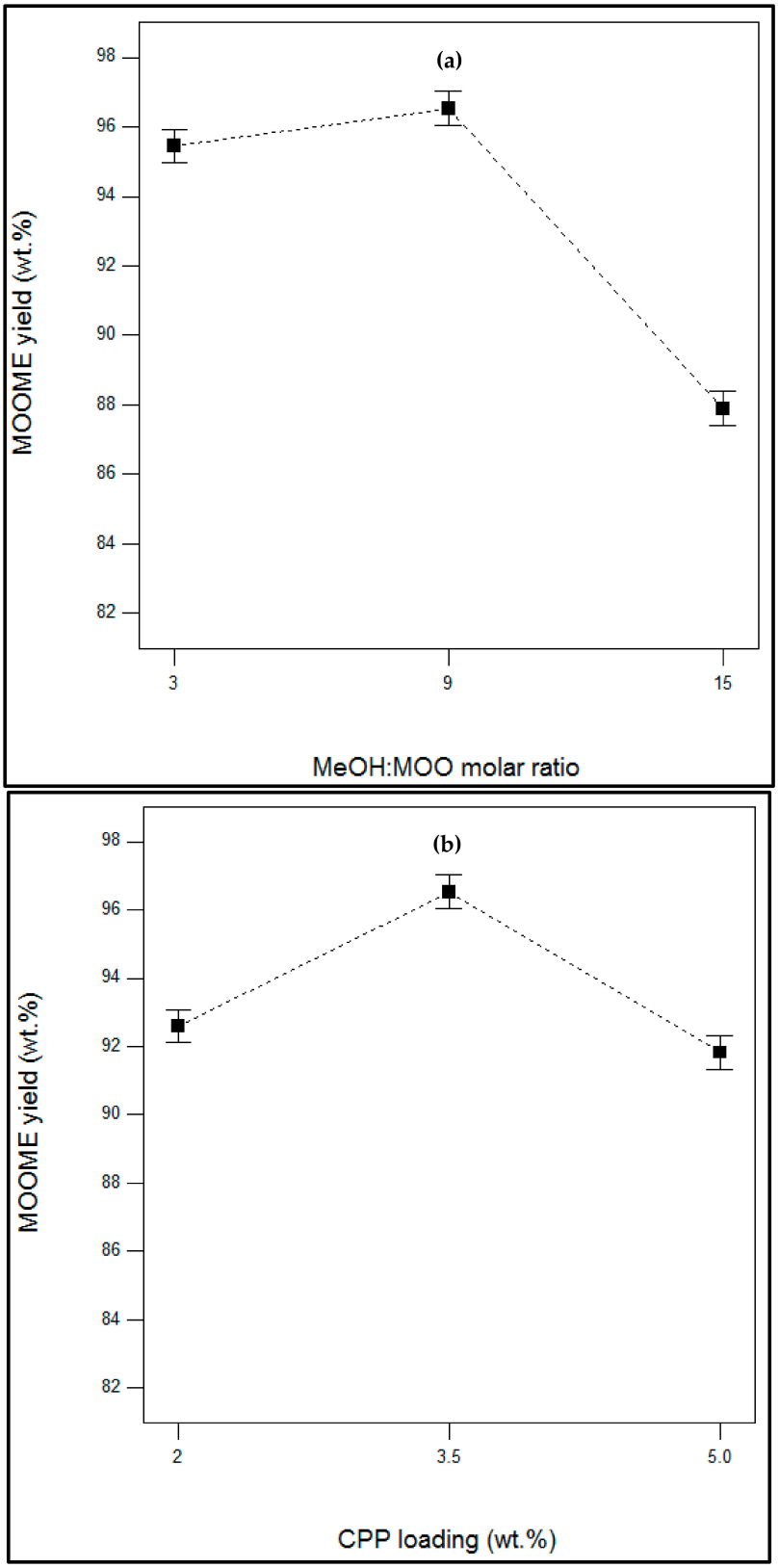

Figure 6. *Cont.*

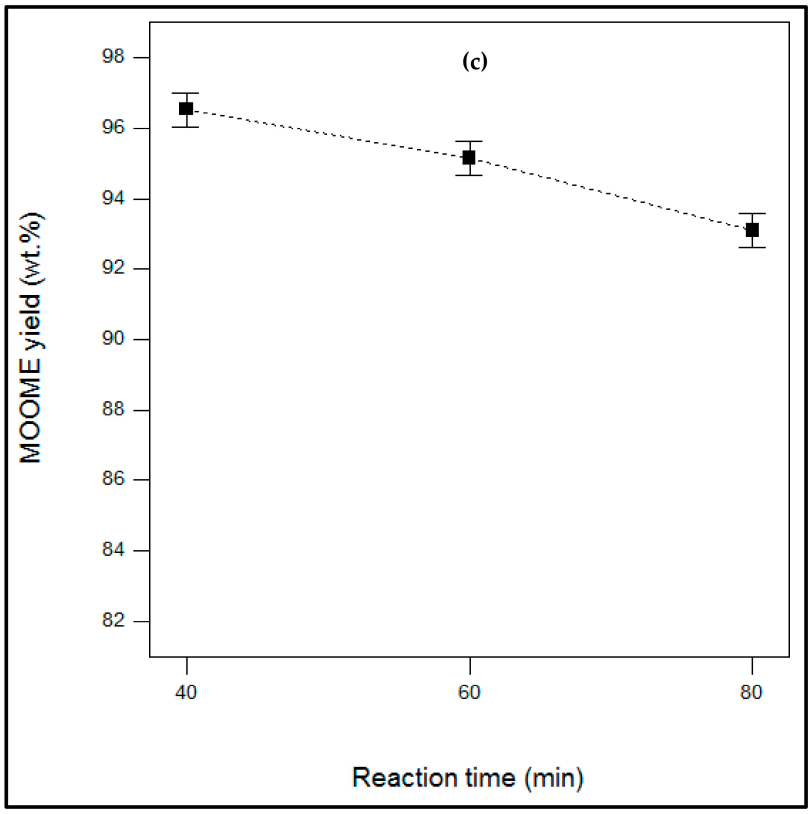

Figure 6. Plots of parametric effect on MOOME yield (**a**) MeOH:MOO molar ratio, (**b**) CPP loading and (**c**) reaction time.

Table 4. Comparison of heterogeneous catalyst characterization, process optimization and biodiesel yield via transesterification.

Source of Triglyceride	Catalyst	Calcination Temperature (°C), Calcination Time (h)	Catalyst Characterization			Process Optimization Conditions				Reusability Cycle (Yield %)	Biodiesel Yield (wt.%)	Reference
			Surface Area (m^2/g)	Pore Volume (cm^3/g)	Pore Diameter (nm)	MeOH:Oil Molar Ratio	Reaction Temperature (°C)	Catalyst Loading (wt.%)	Reaction Time (min)			
Moringa oil	Pawpaw peels	600, 4	3.6042	0.00706	8.54	9:1	35	3.5	40	4 (90.10)	96.43	This study
Moringa oil	$SO_4^{2-}/SnO_2–SiO_2$	300, 2	13.90	0.0403	13.7	1:19.5	150	3	150	-	84	[36]
Moringa oil	KF/eggshell	820, 4	6	0.0556	-	6:1	50	5	60	-	94.2	[37]
Moringa oil	Conch shells	900, 3	1.19	-	-	8.6662:1	65	8.022	130	-	97.06	[38]
Moringa oil	MgO nanocatalyst	-	14.19	0.045	-	12:1	45	1	4	-	93.69	[39]
WCO	*Carica papaya* stem	700, 4	78.681	0.349	3.2148	9:1	60	2	180	5 (85)	95.23	[29]
Kariya oil	Kola nut pod husks	500, 4	5.2199	0.0122	9.3174	6:1	65	3	75	4 (96.28)	98.67	[53]
Sunflower oil	Walnut shell ash	800, 2	8.8	0.000075	<7.5	12:1	60	5	10	4	>98	[63]
Soybean oil	Waste *Brassica nigra* plants	550, 2	7.308	0.011	1.67	12:1	65	7	25	3 (96)	98.79	[64]
Diary waste scum	Waste snail shell	900, 3.5	9.37	0.0538	2.29	12.7:1	58.56	0.866	119.684	5 (86.85)	96.929	[65]
Soybean oil	Banana peels	Open-air burned	1.4546	0.00515	14.1628	6:1	RT	0.7	240	4 (52.16)	98.95	[21]
Soybean oil	Waste snail shell	900, 4	7	0.0312	14.8	6:1	RT	3	420	8 (91)	98	[66]
Jatropha oil	Wood ash	800, 3	3.72	-	-	12:1	65	3	180	-	97.7	[48]
Palm oil	Solid waste peat	600, 2	20.04	0.03155	-	8:1	65	5	90	9 (81.8)	98.6	[67]

WCO—waste cooking oil; RT—room temperature.

3.5. Reusability of CPP Catalyst

One of the benefits of heterogeneous catalysts is their ability to be reused, which can help lower biodiesel production cost in a continuous process. A reusability study of the CPP was carried out using the optimum values predicted. After each experiment, the used CPP catalyst was recovered by centrifugation. The catalyst was then reused with no further treatment (i.e., no cleansing or calcination). Catalysts developed from banana peel [21], walnut shell [63], kola nut pod husk [53], pawpaw stem [29] and elephant-ear tree pod husk [54] have been reported to be recyclable without recalcination of the ashes three, four, four, six and four times, respectively. The MOOME yields observed are 96.53, 94.74, 92.57 and 90.10 wt.% for the first, second, third and fourth cycles, respectively (Figure 7).

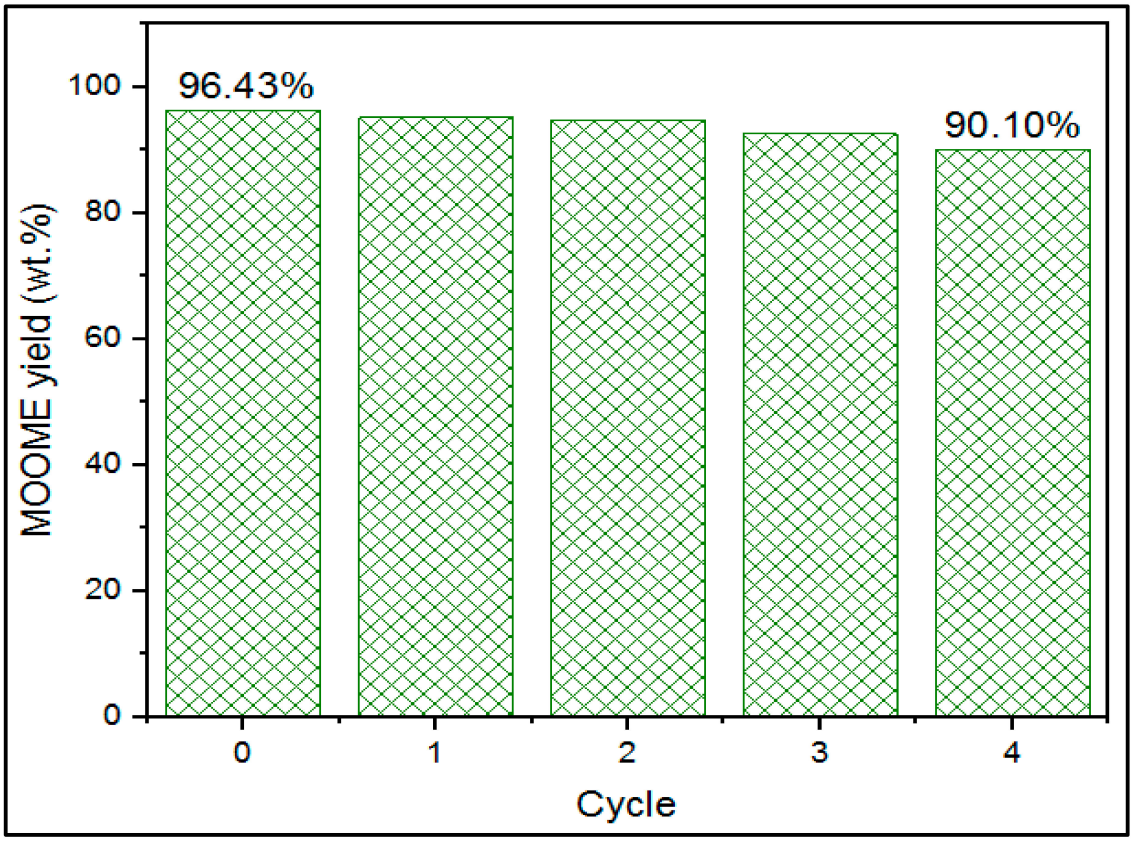

Figure 7. Reusability potential test of CPP.

The percent reduction in the yield after the fourth cycle was 6.7%. The decay in the catalytic activity may be due to the leaching of the CPP into the reacting mixture. A reduction of biodiesel yield of 10.3% was reported for calcined *C. papaya* stem used after the sixth cycle with waste cooking oil [29]. In the work of Falowo et al., a reduction of yield of 24.3% was observed after the fourth cycle when calcined *Enterolobium cyclocarpum* pod husk was used catalyst in the biodiesel production from rubber seed-neem oil mixture [54]. As can be seen in Table 4, a reduction of yield as high as 47.3% was reported when *Musa acuminata* (banana peel) burned in the open air was applied as a catalyst in the biodiesel production from soybean oil [21]. This set of observations demonstrates the efficacy of the CPP developed in this study.

3.6. MOOME Characterization

The physical, chemical, fuel and cold flow qualities of the biodiesel were determined (Table 5). The MOOME produced was a liquid with a golden-brown color (Figure 8). The kinematic viscosity of 4.95 mm^2/s measured in the study shows that the MOOME produced will prevent power failure

caused by the fuel injection pump and injector leakage [68]. The acid value of the MOOME was < 0.5 mg KOH/g oil, which indicates that the biodiesel produced will minimize fuel system deposits with no likelihood of corrosion. The cetane number of 63.05 determined for the methyl esters is higher than the minimum value recommended by ASTM D6751 and EN 14214 for biodiesel. This high value shows that the MOOME had good ignition quality and will minimize the formation of white smoke. The calorific value of the MOOME was 40.70 MJ/kg indicating a sufficient energy capacity in the combustion products, making it attractive clean energy and a potential alternative fuel to diesel. The flash point of the MOOME was measured as 192 °C. This value suggests that the purification method used was effective in the removal of highly volatile impurities, indicating that it can be stored safely at room temperature. The cloud point, pour point and cold filter plugging point, parameters that validate biodiesel applications in low-temperature regions, were 18 and 12 and 10.6 °C, respectively. These values indicate that the MOOME had a high fraction of long-chain saturated fatty acids. The longer the carbon chains in the biodiesel, the poorer the low-temperature properties [69]. The poor cold flow properties of the MOOME observed in this study are noted for biodiesel produced from Moringa oil (Table 5). However, this can be improved using additives such as 2-butyl esters, ethyl acetoacetate, olefin-ester copolymers, ethyl levulinate or polymethyl acrylate [70].

Table 5. MOOME properties based on catalyst influence with reported literature values and biodiesel standards.

Property (unit)	Testing Method	Catalyst									ASTM D6751	EN 14214
		CPP	$NaOCH_3$	$SO_4^{2-}/SnO_2–SiO_2$	KOH	KOH [b]	NaOH	KOH	Nano-MgO	KOH		
Density at 25 °C (kg/m^3)	[71]	877 ± 0.040	-	877.5 [a]	890 [a]	875	-	869.6	880 [a]	859.3	NS	860–900
Kinematic viscosity at 40 °C (mm^2/s)	[71]	4.95 ± 0.000	4.83	4.91	4.78	4.80	4.85	5.05	4.70	5.05	1.9–6.0	3.5–5.0
Acid value (mg KOH/g oil)	[71]	0.224 ± 0.000	-	0.012	0.16	0.38	0.26	0.22	-	-	0.50 max	0.50 max
Calorific value (MJ/kg)	[72]	40.70 ± 0.029	-	-	38.34	45.28	-	40.05	-	40.06	NS	NS
Cetane number	[73]	63.05 ± 0.131	67.07	62.12	63	67	-	-	-	56	47 min	51 min
Flash point (°C)	ASTM D 93	192	-	206	-	162	135	150.5	166	150.1	93 min	101 min
Cloud point (°C)	ASTM D 2500	+18	+18	+10	+10	+18	+18	+19	+15	-	NS	NS
Pour point (°C)	ASTM D 97	+12	+17	+3	+3	+17	+17	+19	+13	-	NS	NS
Cold filter plugging point (°C)	[74]	+10.6	-	-	-	+17	-	+18	-	+39.70	NS	NS
Reference		This study	[31]	[36]	[32]	[75]	[33]	[34]	[39]	[35]		

CPP—calcined pawpaw peels, [a] Conducted at 15 °C, [b] Mean data of the oil seeds value stated, NS—not stated.

Figure 8. Sample of MOOME produced.

The FTIR results for the MOOME produced are illustrated in Figure 9. The band at 3475.84 cm^{-1} in the spectrum is attributed to the overtone of the glyceride ester carbonyl absorption [53,76]. The bands at 2924.18 and 2854.74 cm^{-1} of the spectrum are associated with methyl asymmetric and symmetric stretching vibrations of C–H in CH_2 and CH_3 groups, respectively [46,53]. The strong band at 1745.64 cm^{-1} shows a stretching vibration band of the C=O group of triglycerides [46,53]. The bands illustrated at 1242.20, 1168.90 and 1097.53 cm^{-1} could be ascribed to the C–O group stretching vibrations in esters [46,53]. The overlapping of the methylene rocking vibration and out-of-plane bending vibration of *cis*-disubstituted olefins is presented at 723.33 cm^{-1} [46,53].

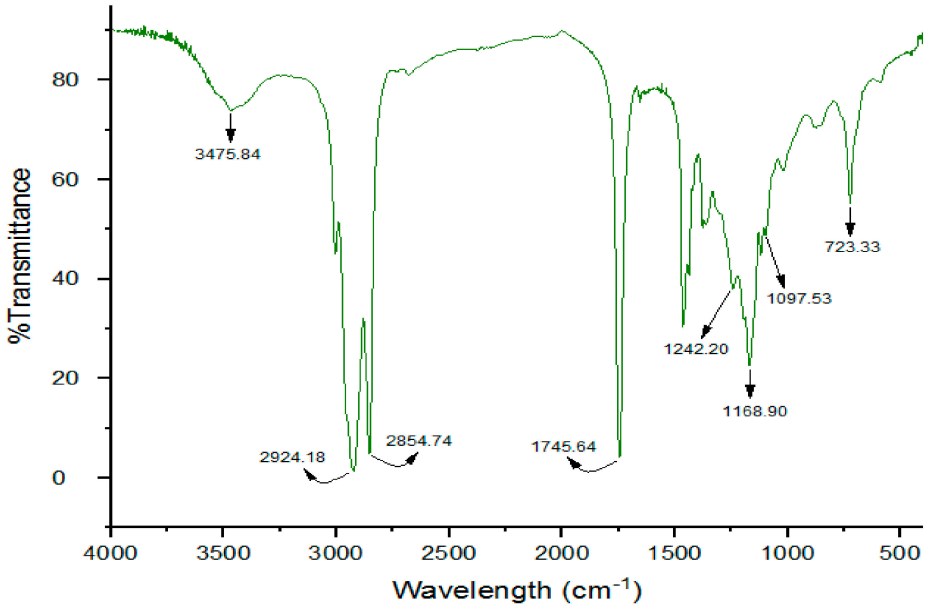

Figure 9. FTIR spectrum of MOOME produced.

3.7. MOOME Production Process Kinetics

For the kinetic modeling in this work, the optimal condition obtained for the transesterification process was used (i.e., 35 °C reaction temperature, 9:1 MeOH:MOO molar ratio, 40 min reaction time and 3.5 wt.% CPP). The conversion of MOO to MOOME with respect to reaction time is illustrated in (Figure 10). The MOOME yield increased rapidly for the first 10 min of the reaction. The rapid MOOME formation observed may be because methyl esters act as a cosolvent in the reaction system since they are easily dissolved in triglycerides and methanol [77]. It was also observed that MOOME production rate slowed down towards the last 10 min as the reaction approached equilibrium. For this present study, the optimum MeOH:MOO molar ratio was 9:1, which implies, $\theta_B = 9$. Based on the densities of MOO (C_{A0}) and MeOH (C_{B0}) (0.887 and 0.792 g/mL, respectively), the initial concentrations of C_{A0} and C_{B0} were determined to be 3.100 and 24.719 mol/L, respectively. The R^2 obtained for the eight scenarios are shown in Table 6. The reaction order with the highest R^2 was selected as the best scenario. The highest R^2 obtained was 0.9926 from Scenario 5 (Table 6). The best fitted kinetic model obtained is expressed by Scenario 5 and the kinetic plot is shown in Figure 11. Therefore, the order of reaction with respect to the reactants, MOO and MeOH were 2 and 0, respectively. Thus, n was determined to be 2 with a corresponding k of 0.20465 $L \cdot mol^{-1} \cdot s^{-1}$, which demonstrates that the transesterification process for MOOME production followed a second-order kinetic model.

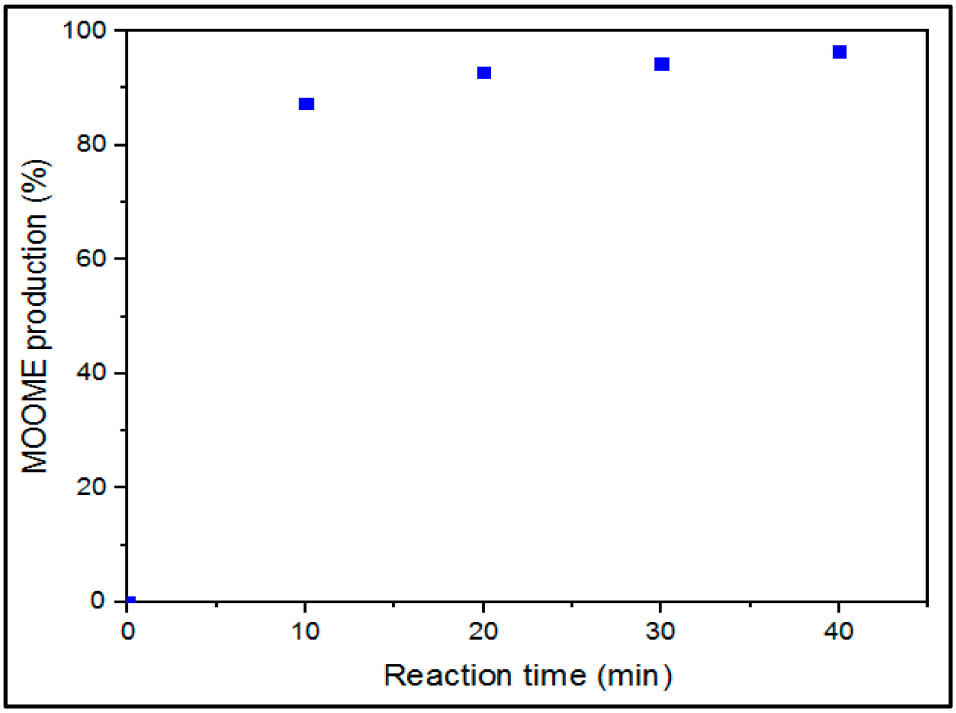

Figure 10. Production plot of MOOME yield against time.

Some previous studies on the transesterification process have demonstrated the kinetics to follow a second-order model [4,78,79], while other authors have reported first-order kinetics using soybean oil [80] and palm oil [41] with heterogeneous metal oxide catalysts. This may be due to the nature of the catalyst employed and the process conditions used, since they tend to influence reaction kinetics.

Table 6. Transesterification kinetics modeling and results.

Scenario	Reaction Order w.r.t. Individual Reactant	Reaction Kinetics Modeling Equation	Overall Reaction Order, n	R^2	k (min^{-1})
1	$\vartheta = 0$, $\mu = 0$	$C_{A0}X = kt$	0	0.8583	0.09729
2	$\vartheta = 1$, $\mu = 0$	$\ln\left[\frac{1}{1-X}\right] = kt$	1	0.9353	0.0975
3	$\vartheta = 0$, $\mu = 1$	$-\frac{1}{3}\left[\ln\frac{\theta_B-3X}{\theta_B}\right] = kt$	1	0.8633	0.00419
4	$\vartheta = 1$, $\mu = 1$	$\frac{1}{C_{A0}(\theta_B-3)}\ln\left[\frac{(\theta_B-3X)}{(1-X)\theta_B}\right] = kt$	2	0.9441	0.00457
5	$\vartheta = 2$, $\mu = 0$	$\frac{X}{C_{A0}(1-X)} = kt$	2	0.9926	0.2047
6	$\vartheta = 0$, $\mu = 2$	$\frac{X}{C_{A0}(\theta_B-3X)\theta_B} = kt$	2	0.8686	1.822×10^{-4}
7	$\vartheta = 2$, $\mu = 1$	$\frac{1}{C_{A0}^2(\theta_B-3)}\left\{\frac{X}{(1-X)} - \frac{3}{(\theta_B-3)}\ln\left[\frac{(\theta_B-3X)}{(1-X)\theta_B}\right]\right\} = kt$	3	0.9912	0.01027
8	$\vartheta = 1$, $\mu = 2$	$\frac{1}{C_{A0}^2(3-\theta_B)}\left\{\frac{3X}{(\theta_B-3X)\theta_B} - \frac{1}{(3-\theta_B)}\ln\left[\frac{(1-X)\theta_B}{(\theta_B-3X)}\right]\right\} = kt$	3	0.9523	2.161×10^{-4}

w.r.t.—with respect to, ϑ—order w.r.t. MOO, μ—order w.r.t. methanol.

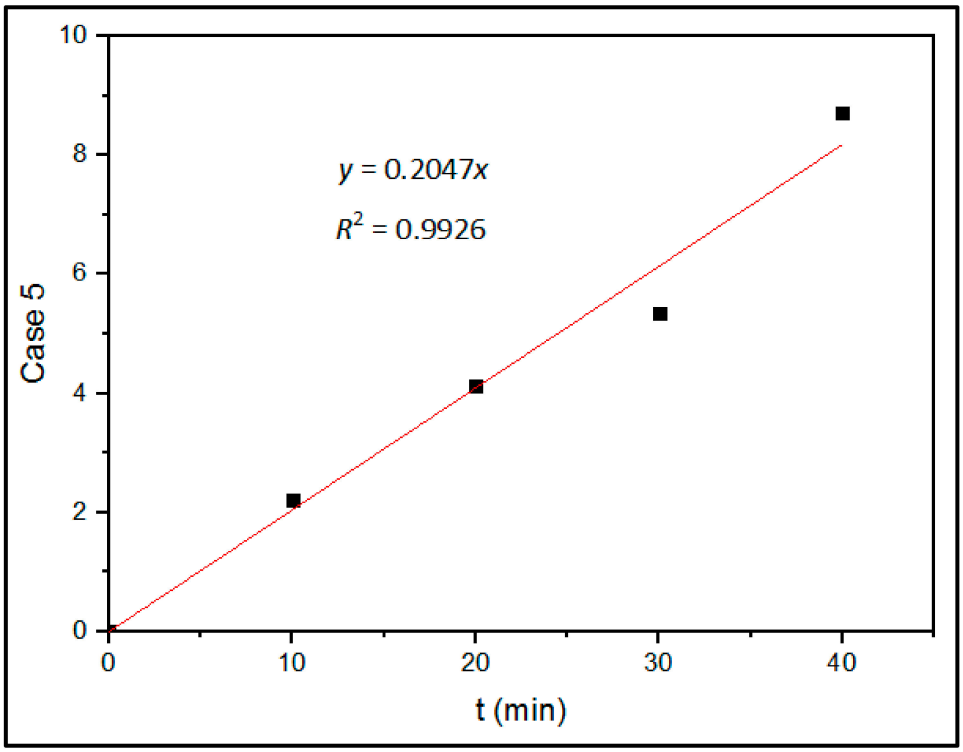

Figure 11. Best-fit kinetic plot for MOOME transesterification.

4. Conclusions

The waste pawpaw peel ash prepared as a solid base catalyst in the present study demonstrated catalytic activity in the conversion of MOO to MOOME by the transesterification process. Characterization of the CPP developed revealed the presence of K, Ca and Mg in significant quantities, which were responsible for the high catalytic activity observed in this study. From the parametric study by the Taguchi method, the optimum values established for the transesterification process were reaction temperature of 35 °C, MeOH:MOO molar ratio of 9:1, reaction time of 40 min and CPP loading of 3.5 wt.% with a MOOME yield of 96.43 ± 0.10 wt.%. MeOH:MOO molar ratio had the highest significant effect on the MOOME yield with an impact factor of 70.28%. The quality of the MOOME produced showed the feasibility of its application as a low-cost energy resource and environmentally benign fuel in diesel engines. The kinetic data obtained were an overall reaction order of 2 and a reaction rate constant of 0.20465 $L \cdot mol^{-1} \cdot s^{-1}$. Thus, it could be concluded that waste pawpaw peel and moringa oil could be used to produce quality biodiesel that meets biodiesel standard specifications.

Author Contributions: Conceptualization, E.B. and T.V.O.; methodology, E.B. and B.O.; software, E.B. and B.O.; validation, E.B. and B.O.; formal analysis, B.O.; investigation, B.O.; resources, E.B., T.V.O. and L.M.L.; data curation, E.B. and B.O.; writing—original draft preparation, B.O.; writing—review and editing, E.B., T.V.O. and L.M.L; visualization, E.B and B.O.; supervision, E.B. and T.V.O.; project administration, E.B. and T.V.O. All authors have read and agreed to the published version of the manuscript.

Funding: This research received no external funding and The APC was funded by [Cape Peninsula University of Technology].

Acknowledgments: E.B. acknowledges the working environment provided by FAMU in the course of developing the manuscript. Assistance offered by Miriam de Almeida in the catalyst analysis is acknowledged.

Conflicts of Interest: The authors declare no conflict of interest.

Abbreviations

ANOVA	Analysis of variance
BET	Brunauer–Emmett–Teller
BJH	Brunauer–Joyner–Halenda
CPP	Calcined pawpaw peels
EDX	Energy-dispersive X-ray spectroscopy
FTIR	Fourier transform infrared
MOO	*Moringa oleifera* oil
MOOME	*Moringa oleifera* oil methyl esters
R^2	Coefficient of determination
RPP	Raw pawpaw peel
SEM	Scanning electron microscopy
SNR	Signal-to-noise ratio
XRD	X-ray diffraction

References

1. Abdullah, S.H.Y.S.; Hanapi, N.H.M.; Azid, A.; Umar, R.; Juahir, H.; Khatoon, H.; Endut, A. A review of biomass-derived heterogeneous catalyst for a sustainable biodiesel production. *Renew. Sustain. Energy Rev.* **2017**, *70*, 1040–1051. [CrossRef]
2. Leung, D.Y.; Wu, X.; Leung, M. A review on biodiesel production using catalyzed transesterification. *Appl. Energy* **2010**, *87*, 1083–1095. [CrossRef]
3. Odude, V.O.; Adesina, A.J.; Oyetunde, O.O.; Adeyemi, O.O.; Ishola, N.B.; Etim, A.O.; Betiku, E. Application of agricultural waste-based catalysts to transesterification of esterified palm kernel oil into biodiesel: A case of banana fruit peel versus cocoa pod husk. *Waste and Biomass Valoriz.* **2019**, *10*, 877–888. [CrossRef]
4. Stamenković, O.S.; Todorović, Z.B.; Lazić, M.L.; Veljković, V.B.; Skala, D.U. Kinetics of sunflower oil methanolysis at low temperatures. *Bioresour. Technol.* **2008**, *99*, 1131–1140. [CrossRef] [PubMed]
5. Likozar, B.; Levec, J. Effect of process conditions on equilibrium, reaction kinetics and mass transfer for triglyceride transesterification to biodiesel: Experimental and modeling based on fatty acid composition. *Fuel Process. Technol.* **2014**, *122*, 30–41. [CrossRef]
6. Negm, N.A.; Sayed, G.H.; Yehia, F.Z.; Habib, O.I.; Mohamed, E.A. Biodiesel production from one-step heterogeneous catalyzed process of castor oil and jatropha oil using novel sulphonated phenyl silane montmorillonite catalyst. *J. Mol. Liq.* **2017**, *234*, 157–163. [CrossRef]
7. Betiku, E.; Etim, A.O.; Pereao, O.; Ojumu, T.V. Two-step conversion of neem (*Azadirachta indica*) seed oil into fatty methyl esters using an heterogeneous biomass-based catalyst: An example of cocoa pod husk. *Energy Fuels* **2017**, *31*, 6182–6193. [CrossRef]
8. Vadery, V.; Narayanan, B.N.; Ramakrishnan, R.M.; Cherikkallinmel, S.K.; Sugunan, S.; Narayanan, D.P.; Sasidharan, S. Room temperature production of jatropha biodiesel over coconut husk ash. *Energy* **2014**, *70*, 588–594. [CrossRef]
9. Silitonga, A.; Mahlia, T.; Kusumo, F.; Dharma, S.; Sebayang, A.; Sembiring, R.; Shamsuddin, A. Intensification of reutealis trisperma biodiesel production using infrared radiation: Simulation, optimisation and validation. *Renew. Energy* **2019**, *133*, 520–527. [CrossRef]
10. Silitonga, A.; Shamsuddin, A.; Mahlia, T.; Milano, J.; Kusumo, F.; Siswantoro, J.; Dharma, S.; Sebayang, A.; Masjuki, H.; Ong, H.C. Biodiesel synthesis from *Ceiba pentandra* oil by microwave irradiation-assisted transesterification: ELM modeling and optimization. *Renew. Energy* **2020**, *146*, 1278–1291. [CrossRef]
11. Ong, H.C.; Milano, J.; Silitonga, A.S.; Hassan, M.H.; Wang, C.-T.; Mahlia, T.M.I.; Siswantoro, J.; Kusumo, F.; Sutrisno, J. Biodiesel production from *Calophyllum inophyllum-Ceiba pentandra* oil mixture: Optimization and characterization. *J. Clean. Prod.* **2019**, *219*, 183–198. [CrossRef]
12. Oraegbunam, J.C.; Oladipo, B.; Falowo, O.A.; Betiku, E. Clean sandbox (*Hura crepitans*) oil methyl esters synthesis: A kinetic and thermodynamic study through pH monitoring approach. *Renew. Energy* **2020**, *160*, 526–537.

13. Tan, Y.H.; Abdullah, M.O.; Nolasco-Hipolito, C.; Taufiq-Yap, Y.H. Waste ostrich-and chicken-eggshells as heterogeneous base catalyst for biodiesel production from used cooking oil: Catalyst characterization and biodiesel yield performance. *Appl. Energy* **2015**, *160*, 58–70. [CrossRef]
14. Hossain, A.S.; Salleh, A.; Boyce, A.N.; Chowdhury, P.; Naqiuddin, M. Biodiesel fuel production from algae as renewable energy. *Am. J. Biochem. Biotechnol.* **2008**, *4*, 250–254. [CrossRef]
15. Srivastava, A.; Prasad, R. Triglycerides-based diesel fuels. *Renew. Sustain. Energy Rev.* **2000**, *4*, 111–133. [CrossRef]
16. Boro, J.; Thakur, A.J.; Deka, D. Solid oxide derived from waste shells of *Turbonilla striatula* as a renewable catalyst for biodiesel production. *Fuel Process. Technol.* **2011**, *92*, 2061–2067. [CrossRef]
17. Pinto, A.C.; Guarieiro, L.L.; Rezende, M.J.; Ribeiro, N.M.; Torres, E.A.; Lopes, W.A.; Pereira, P.A.d.P.; Andrade, J.B.d. Biodiesel: An overview. *J. Braz. Chem. Soc.* **2005**, *16*, 1313–1330. [CrossRef]
18. Dhawane, S.H.; Kumar, T.; Halder, G. Biodiesel synthesis from *Hevea brasiliensis* oil employing carbon supported heterogeneous catalyst: Optimization by Taguchi method. *Renew. Energy* **2016**, *89*, 506–514. [CrossRef]
19. Betiku, E.; Akintunde, A.M.; Ojumu, T.V. Banana peels as a biobase catalyst for fatty acid methyl esters production using napoleon's plume (*Bauhinia monandra*) seed oil: A process parameters optimization study. *Energy* **2016**, *103*, 797–806. [CrossRef]
20. Gohain, M.; Devi, A.; Deka, D. *Musa balbisiana* colla peel as highly effective renewable heterogeneous base catalyst for biodiesel production. *Ind. Crops. Prods.* **2017**, *109*, 8–18. [CrossRef]
21. Pathak, G.; Das, D.; Rajkumari, K.; Rokhum, L. Exploiting waste: Towards a sustainable production of biodiesel using *Musa acuminata* peel ash as a heterogeneous catalyst. *Green Chem.* **2018**, *20*, 2365–2373. [CrossRef]
22. Onoji, S.E.; Iyuke, S.E.; Igbafe, A.I.; Daramola, M.O. Transesterification of rubber seed oil to biodiesel over a calcined waste rubber seed shell catalyst: Modeling and optimization of process variables. *Energy Fuels* **2017**, *31*, 6109–6119. [CrossRef]
23. Mendonça, I.M.; Paes, O.A.; Maia, P.J.; Souza, M.P.; Almeida, R.A.; Silva, C.C.; Duvoisin, S., Jr.; de Freitas, F.A. New heterogeneous catalyst for biodiesel production from waste tucumã peels (*Astrocaryum aculeatum* meyer): Parameters optimization study. *Renew. Energy* **2019**, *130*, 103–110. [CrossRef]
24. Zhao, C.; Lv, P.; Yang, L.; Xing, S.; Luo, W.; Wang, Z. Biodiesel synthesis over biochar-based catalyst from biomass waste pomelo peel. *Energy Convers. Manag.* **2018**, *160*, 477–485. [CrossRef]
25. Etim, A.O.; Betiku, E.; Ajala, S.O.; Olaniyi, P.J.; Ojumu, T.V. Potential of ripe plantain fruit peels as an ecofriendly catalyst for biodiesel synthesis: Optimization by artificial neural network integrated with genetic algorithm. *Sustainability* **2018**, *10*, 707. [CrossRef]
26. Medina, J.; Gutiérrez, G.V.; García, H. Pawpaw: Post-harvest Operation. Compendium on Post-harvest Operations. Available online: http://www.fao.org/fileadmin/user_upload/inpho/docs/Post_Harvest_Compendium_-_Pawpaw__Papaya_.pdf (accessed on 15 September 2019).
27. Evans, E.A.; Ballen, F.H. *An Overview of Global Papaya Production, Trade, and Consumption*; University of Florida: Gainesville, FL, USA, 2012.
28. FAOSTAT. Statistical Databases. Food and Agriculture Organization of the United Nations. Statistics Division 2016. Available online: www.fao.org/faostat/en/#data/QC (accessed on 23 January 2018).
29. Gohain, M.; Laskar, K.; Paul, A.K.; Daimary, N.; Maharana, M.; Goswami, I.K.; Hazarika, A.; Bora, U.; Deka, D. *Carica papaya* stem: A source of versatile heterogeneous catalyst for biodiesel production and c–c bond formation. *Renew. Energy* **2020**, *147*, 541–555. [CrossRef]
30. Oladipo, B.; Betiku, E. Process optimization of solvent extraction of seed oil from *Moringa oleifera*: An appraisal of quantitative and qualitative process variables on oil quality using d-optimal design. *Biocatal. Agric. Biotechnol.* **2019**, *20*, 101187. [CrossRef]
31. Rashid, U.; Anwar, F.; Moser, B.R.; Knothe, G. *Moringa oleifera* oil: A possible source of biodiesel. *Bioresour. Technol.* **2008**, *99*, 8175–8179. [CrossRef]
32. Kivevele, T.T.; Mbarawa, M.M.; Bereczky, A.K.; Zoöldy, M.T. Evaluation of the oxidation stability of biodiesel produced from *Moringa oleifera* oil. *Energy Fuels* **2011**, *25*, 5416–5421.
33. Zubairu, A.; Ibrahim, F.S. *Moringa oleifera* oilseed as viable feedstock for biodiesel production in northern Nigeria. *Int. J. Energy Eng.* **2014**, *4*, 21–25.

34. Mofijur, M.; Masjuki, H.; Kalam, M.; Rasul, M.; Atabani, A.E.; Hazrat, M.; Mahmudul, H. Effect of biodiesel-diesel blending on physico-chemical properties of biodiesel produced from *Moringa oleifera*. *Proc. Eng.* **2015**, *105*, 665–669. [CrossRef]
35. Karthickeyan, V. Effect of cetane enhancer on *Moringa oleifera* biodiesel in a thermal coated direct injection diesel engine. *Fuel* **2019**, *235*, 538–550. [CrossRef]
36. Kafuku, G.; Lam, M.K.; Kansedo, J.; Lee, K.T.; Mbarawa, M. Heterogeneous catalyzed biodiesel production from *Moringa oleifera* oil. *Fuel Process. Technol.* **2010**, *91*, 1525–1529. [CrossRef]
37. Aziz, M.; Triwahyono, S.; Jalil, A.; Rapai, H.; Atabani, A. Transesterification of *Moringa oleifera* oil to biodiesel using potassium flouride loaded eggshell as catalyst. *Malays. J. Catal.* **2016**, *1*, 22–26.
38. Niju, S.; Anushya, C.; Balajii, M. Process optimization for biodiesel production from *Moringa oleifera* oil using conch shells as heterogeneous catalyst. *Environ. Prog. Sustain. Energy* **2019**, *38*, e13015. [CrossRef]
39. Esmaeili, H.; Yeganeh, G.; Esmaeilzadeh, F. Optimization of biodiesel production from *Moringa oleifera* seeds oil in the presence of nano-mgo using taguchi method. *Int. Nano Lett.* **2019**, *9*, 257–263. [CrossRef]
40. Ighose, B.O.; Adeleke, I.A.; Damos, M.; Junaid, H.A.; Okpalaeke, K.E.; Betiku, E. Optimization of biodiesel production from *Thevetia peruviana* seed oil by adaptive neuro-fuzzy inference system coupled with genetic algorithm and response surface methodology. *Energy Convers. Manag.* **2017**, *132*, 231–240. [CrossRef]
41. Ye, W.; Gao, Y.; Ding, H.; Liu, M.; Liu, S.; Han, X.; Qi, J. Kinetics of transesterification of palm oil under conventional heating and microwave irradiation, using cao as heterogeneous catalyst. *Fuel* **2016**, *180*, 574–579. [CrossRef]
42. Oladipo, B.; Betiku, E. Optimization and kinetic studies on conversion of rubber seed (*Hevea brasiliensis*) oil to methyl esters over a green biowaste catalyst. *J. Environ. Manag.* **2020**, *268*, 110705.
43. Hameed, B.H.; Lai, L.; Chin, L. Production of biodiesel from palm oil (*Elaeis guineensis*) using heterogeneous catalyst: An optimized process. *Fuel Process. Technol.* **2009**, *90*, 606–610. [CrossRef]
44. Kumar, D.; Ali, A. Nanocrystalline k–cao for the transesterification of a variety of feedstocks: Structure, kinetics and catalytic properties. *Biomass Bioenergy* **2012**, *46*, 459–468. [CrossRef]
45. Sarmah, M.; Dewan, A.; Mondal, M.; Thakur, A.J.; Bora, U. Analysis of the water extract of waste papaya bark ash and its implications as an in situ base in the ligand-free recyclable suzuki–miyaura coupling reaction. *RSC Adv.* **2016**, *6*, 28981–28985. [CrossRef]
46. Nath, B.; Kalita, P.; Das, B.; Basumatary, S. Highly efficient renewable heterogeneous base catalyst derived from waste *Sesamum indicum* plant for synthesis of biodiesel. *Renew. Energy* **2020**, *151*, 295–310. [CrossRef]
47. Betiku, E.; Ajala, S.O. Modeling and optimization of *Thevetia peruviana* (yellow oleander) oil biodiesel synthesis via *Musa paradisiaca* (plantain) peels as heterogeneous base catalyst: A case of artificial neural network vs. Response surface methodology. *Ind. Crops. Prods.* **2014**, *53*, 314–322. [CrossRef]
48. Sharma, M.; Khan, A.A.; Puri, S.; Tuli, D. Wood ash as a potential heterogeneous catalyst for biodiesel synthesis. *Biomass Bioenergy* **2012**, *41*, 94–106. [CrossRef]
49. Coates, J. Interpretation of Infrared Spectra, A Practical Approach. In *Encyclopedia of Analytical Chemistry*; John Wiley & Sons Ltd: Chichester, UK, 2000; pp. 10815–10837.
50. Yamaguchi, T.; Wang, Y.; Komatsu, M.; Ookawa, M. Preparation of new solid bases derived from supported metal nitrates and carbonates. *Catal. Surv. Jpn.* **2002**, *5*, 81–89. [CrossRef]
51. Basumatary, S.; Nath, B.; Das, B.; Kalita, P.; Basumatary, B. Utilization of renewable and sustainable basic heterogeneous catalyst from *Heteropanax fragrans* (Kesseru) for effective synthesis of biodiesel from *Jatropha curcas* oil. *Fuel* **2021**, *286*, 119357. [CrossRef]
52. Falowo, O.A.; Ojumu, T.V.; Pereao, O.; Betiku, E. Sustainable biodiesel synthesis from honne-rubber-neem oil blend with a novel mesoporous base catalyst synthesized from a mixture of three agrowastes. *Catalysts* **2020**, *10*, 190. [CrossRef]
53. Betiku, E.; Okeleye, A.A.; Ishola, N.B.; Osunleke, A.S.; Ojumu, T.V. Development of a novel mesoporous biocatalyst derived from kola nut pod husk for conversion of kariya seed oil to methyl esters: A case of synthesis, modeling and optimization studies. *Catal. Lett.* **2019**, *149*, 1772–1787. [CrossRef]
54. Falowo, O.A.; Oloko-Oba, M.I.; Betiku, E. Biodiesel production intensification via microwave irradiation-assisted transesterification of oil blend using nanoparticles from elephant-ear tree pod husk as a base heterogeneous catalyst. *Chem. Eng. Process. Process Intensif.* **2019**, *140*, 157–170. [CrossRef]
55. Sing, K.S. Reporting physisorption data for gas/solid systems with special reference to the determination of surface area and porosity (recommendations 1984). *Pure Appl. Chem.* **1985**, *57*, 603–619. [CrossRef]

56. Shan, R.; Chen, G.; Yan, B.; Shi, J.; Liu, C. Porous cao-based catalyst derived from pss-induced mineralization for biodiesel production enhancement. *Energy Convers. Manag.* **2015**, *106*, 405–413. [CrossRef]
57. Myers, R.H.; Montgomery, D.C.; Anderson-Cook, C. *Response Surface Methodology: Product and Process Optimization Using Designed Experiments*; John Wiley & Sons: New York, NY, USA, 2009.
58. Knothe, G.; Razon, L.F. Biodiesel fuels. *Prog. Energy Combust. Sci.* **2017**, *58*, 36–59. [CrossRef]
59. Ahmad, J.; Yusup, S.; Bokhari, A.; Kamil, R.N.M. Study of fuel properties of rubber seed oil based biodiesel. *Energy Convers. Manag.* **2014**, *78*, 266–275. [CrossRef]
60. Lv, Y.; Sun, S.; Liu, J. Biodiesel production catalyzed by a methanol-tolerant lipase a from *Candida antarctica* in the presence of excess water. *ACS Omega* **2019**, *4*, 20064–20071. [CrossRef]
61. Leung, D.Y.C.; Guo, Y. Transesterification of neat and used frying oil: Optimization for biodiesel production. *Fuel Process. Technol.* **2006**, *87*, 883–890. [CrossRef]
62. Abu-Jrai, A.M.; Jamil, F.; Ala'a, H.; Baawain, M.; Al-Haj, L.; Al-Hinai, M.; Al-Abri, M.; Rafiq, S. Valorization of waste date pits biomass for biodiesel production in presence of green carbon catalyst. *Energy Convers. Manag.* **2017**, *135*, 236–243. [CrossRef]
63. Miladinović, M.R.; Zdujić, M.V.; Veljović, D.N.; Krstić, J.B.; Banković-Ilić, I.B.; Veljković, V.B.; Stamenković, O.S. Valorization of walnut shell ash as a catalyst for biodiesel production. *Renew. Energy* **2020**, *147*, 1033–1043. [CrossRef]
64. Nath, B.; Das, B.; Kalita, P.; Basumatary, S. Waste to value addition: Utilization of waste *Brassica nigra* plant derived novel green heterogeneous base catalyst for effective synthesis of biodiesel. *J. Clean. Prod.* **2019**, *239*, 118112. [CrossRef]
65. Krishnamurthy, K.; Sridhara, S.; Kumar, C.A. Optimization and kinetic study of biodiesel production from *Hydnocarpus wightiana* oil and dairy waste scum using snail shell cao nano catalyst. *Renew. Energy* **2020**, *146*, 280–296. [CrossRef]
66. Laskar, I.B.; Rajkumari, K.; Gupta, R.; Chatterjee, S.; Paul, B.; Rokhum, L. Waste snail shell derived heterogeneous catalyst for biodiesel production by the transesterification of soybean oil. *RSC Adv.* **2018**, *8*, 20131–20142. [CrossRef]
67. Wang, S.; Zhao, C.; Shan, R.; Wang, Y.; Yuan, H. A novel peat biochar supported catalyst for the transesterification reaction. *Energy Convers. Manag.* **2017**, *139*, 89–96. [CrossRef]
68. Suthisripok, T.; Semsamran, P. The impact of biodiesel b100 on a small agricultural diesel engine. *Tribol. Int.* **2018**, *128*, 397–409. [CrossRef]
69. Wu, M.; Wu, G.; Han, L.; Wang, J. Low-temperature fluidity of biodiesel fuel prepared from edible vegetable oil. *Pet. Process. Petrochem.* **2005**, *36*, 57–60.
70. Verma, P.; Sharma, M.; Dwivedi, G. Evaluation and enhancement of cold flow properties of palm oil and its biodiesel. *Energy Rep.* **2016**, *2*, 8–13. [CrossRef]
71. AOAC. *Official Methods of Analysis of the Association of Official Analytical Chemists*; AOAC: Washington, DC, USA, 1990.
72. Demirbaş, A. Fuel properties and calculation of higher heating values of vegetable oils. *Fuel* **1998**, *77*, 1117–1120. [CrossRef]
73. Krisnangkura, K. A simple method for estimation of cetane index of vegetable oil methyl esters. *J. Am. Oil Chem. Soc.* **1986**, *63*, 552–553. [CrossRef]
74. Sharafutdinov, I.; Stratiev, D.; Shishkova, I.; Dinkov, R.; Batchvarov, A.; Petkov, P.; Rudnev, N. Cold flow properties and oxidation stability of blends of near zero sulfur diesel from ural crude oil and fame from different origin. *Fuel* **2012**, *96*, 556–567. [CrossRef]
75. Rashid, U.; Anwar, F.; Ashraf, M.; Saleem, M.; Yusup, S. Application of response surface methodology for optimizing transesterification of *Moringa oleifera* oil: Biodiesel production. *Energy Convers. Manag.* **2011**, *52*, 3034–3042. [CrossRef]
76. Guillén, M.D.; Cabo, N. Relationships between the composition of edible oils and lard and the ratio of the absorbance of specific bands of their fourier transform infrared spectra. Role of some bands of the fingerprint region. *J. Agric. Food Chem.* **1998**, *46*, 1788–1793. [CrossRef]
77. Stamenković, O.S.; Lazić, M.; Todorović, Z.; Veljković, V.; Skala, D. The effect of agitation intensity on alkali-catalyzed methanolysis of sunflower oil. *Bioresour. Technol.* **2007**, *98*, 2688–2699. [CrossRef]
78. Darnoko, D.; Cheryan, M. Kinetics of palm oil transesterification in a batch reactor. *J. Am. Oil Chem. Soc.* **2000**, *77*, 1263–1267. [CrossRef]

79. Foon, C.S.; May, C.Y.; Ngan, M.A.; Hock, C.C. Kinetics study on transesterification of palm oil. *J. Oil Palm Res.* **2004**, *16*, 19–29.
80. Singh, A.K.; Fernando, S.D. Reaction kinetics of soybean oil transesterification using heterogeneous metal oxide catalysts. *Chem. Eng. Technol.* **2007**, *30*, 1716–1720. [CrossRef]